New Phytologist

The tomato cytochrome P450 CYP712G1 catalyses the double oxidation of orobanchol *en route* to the rhizosphere signalling strigolactone, solanacol

Yanting Wang[1], Janani Durairaj[2], Hernando G. Suárez Duran[2], Robin van Velzen[3], Kristyna Flokova[1], Che-Yang Liao[1,4], Aleksandra Chojnacka[1], Stuart MacFarlane[5], M. Eric Schranz[3], Marnix H. Medema[2], Aalt D. J. van Dijk[2], Lemeng Dong[1] and Harro J. Bouwmeester[1]

[1]Plant Hormone Biology Group, Swammerdam Institute for Life Sciences, University of Amsterdam, Science Park 904, 1098 XH Amsterdam, the Netherlands; [2]Bioinformatics Group, Wageningen University, 6708PB Wageningen, the Netherlands; [3]Biosystematics Group, Wageningen University, 6708PB Wageningen, the Netherlands; [4]Plant Ecophysiology, Institute of Environmental Biology, Utrecht University, 3584 CH Utrecht, the Netherlands; [5]Cell and Molecular Sciences, the James Hutton Institute, Invergowrie, Dundee, DD2 5DA, UK

Author for correspondence:
Harro J. Bouwmeester
Email: h.j.bouwmeester@uva.nl

Received: *16 February 2022*
Accepted: *9 May 2022*

New Phytologist (2022) **235:** 1884–1899
doi: 10.1111/nph.18272

Key words: CYP712G1, orobanchol, oxidation, solanacol, strigolactone biosynthesis, tomato (*Solanum lycopersicum*).

Summary

- Strigolactones (SLs) are rhizosphere signalling molecules and phytohormones. The biosynthetic pathway of SLs in tomato has been partially elucidated, but the structural diversity in tomato SLs predicts that additional biosynthetic steps are required. Here, root RNA-seq data and co-expression analysis were used for SL biosynthetic gene discovery.
- This strategy resulted in a candidate gene list containing several cytochrome P450s. Heterologous expression in *Nicotiana benthamiana* and yeast showed that one of these, CYP712G1, can catalyse the double oxidation of orobanchol, resulting in the formation of three didehydro-orobanchol (DDH) isomers.
- Virus-induced gene silencing and heterologous expression in yeast showed that one of these DDH isomers is converted to solanacol, one of the most abundant SLs in tomato root exudate. Protein modelling and substrate docking analysis suggest that hydroxy-orbanchol is the likely intermediate in the conversion from orobanchol to the DDH isomers.
- Phylogenetic analysis demonstrated the occurrence of CYP712G1 homologues in the Eudicots only, which fits with the reports on DDH isomers in that clade. Protein modelling and orobanchol docking of the putative tobacco CYP712G1 homologue suggest that it can convert orobanchol to similar DDH isomers as tomato.

Introduction

Strigolactones (SLs) were initially discovered as germination stimulants that induce the seed germination of parasitic plants of the Orobanchaceae (*Striga*, *Alectra*, *Phelipanche* and *Orobanche* genera) (Cook *et al.*, 1966; Bouwmeester *et al.*, 2020). Half a century after this intriguing biological discovery, it was demonstrated that SLs are actually beneficial for plants, as they induce hyphal branching in arbuscular mycorrhizal (AM) fungi (Akiyama *et al.*, 2005). Another 3 yr later, SLs were revealed to be a class of plant hormones regulating plant architecture and development (Gomez-Roldan *et al.*, 2008; Umehara *et al.*, 2008; Ruyter-Spira *et al.*, 2011; Kapulnik & Koltai, 2014; Sun *et al.*, 2015).

Interestingly, substantial structural diversification has occurred in the SLs, between as well as within plant species. So far *c.* 30 different SLs have been reported and individual plant species have been reported to exude up to 11 different SLs (Xie, 2016; Wang & Bouwmeester, 2018; Xie *et al.*, 2019). SLs can be classified into canonical and noncanonical SLs that all have the butenolide D-ring responsible for their biological activity. Different SLs may have different biological activities with regard to seed germination stimulation of parasitic plants, hyphal branching of AM fungi and hormonal activity (Akiyama *et al.*, 2010; Boyer *et al.*, 2012; Nomura *et al.*, 2013; Zwanenburg & Pospíšil, 2013). Possibly, these different functions have driven the structural diversification in the SLs, with biological specificity in beneficial signalling relationships as fitness traits. Knowledge of the biosynthesis of these different SLs should shed more light on their biological relevance.

The biosynthesis of SLs so far has only been partially unravelled, and mainly in model plants. The core SL biosynthetic pathway involves the enzymes DWARF27 (D27), CAROTENOID CLEAVAGE DIOXYGENASE 7 (CCD7) and CAROTENOID CLEAVAGE DIOXYGENASE 8 (CCD8) (Fig. 1) (Morris *et al.*, 2001; Sorefan *et al.*, 2003; Zou *et al.*, 2006; Arite *et al.*, 2007; Simons *et al.*, 2007; Drummond *et al.*, 2009; Lin *et al.*, 2009; Alder *et al.*, 2012). These three proteins can sequentially convert β-carotene into carlactone, which seems to be the common precursor

© 2022 The Authors
New Phytologist © *2022 New Phytologist Foundation.*
This is an open access article under the terms of the Creative Commons Attribution-NonCommercial License, which permits use, distribution and reproduction in any medium, provided the original work is properly cited and is not used for commercial purposes.

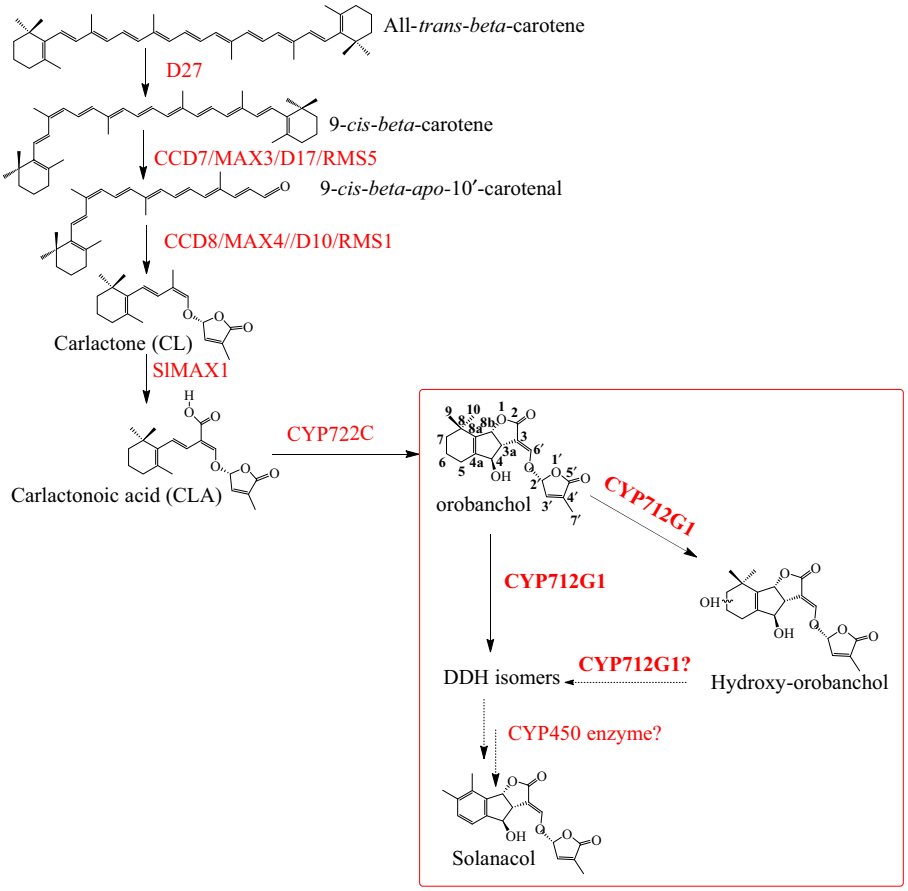

Fig. 1 The proposed strigolactone (SL) biosynthetic pathway in tomato (*Solanum lycopersicum*). Elucidated steps are indicated with solid and putative steps with broken arrows. The proposed structures of didehydro-orobanchol (DDH) isomers are shown in Supporting Information Fig. S8.

for all SLs (Alder *et al.*, 2012). In Arabidopsis, MORE AXILLARY GROWTH 1 (MAX1) can convert carlactone (CL) into carlactonoic acid (CLA) (Abe *et al.*, 2014; Seto *et al.*, 2014; Xu *et al.*, 2021). In rice, two MAX1 homologues convert CL into 4-deoxyorobanchol (4-DO) (CL oxidase) and 4-DO into orobanchol (4-DO hydroxylase) (Zhang *et al.*, 2014).

In tomato, the SL biosynthetic pathway has been partially resolved, with the characterisation of *CCD7* and *CCD8* (Vogel *et al.*, 2010; Kohlen *et al.*, 2012; Zhang *et al.*, 2018). Two cytochrome P450s, the MAX1 homologue SlMAX1 and CYP722C, sequentially convert CL into CLA and CLA into orobanchol, respectively (Zhang *et al.*, 2018; Wakabayashi *et al.*, 2019). However, tomato exudes many different SLs, such as orobanchol, solanacol, several didehydro-orobanchol (DDH) isomers, orobanchyl acetate, 7-oxo-orobanchol and 7-hydroxy-orobanchol (Koltai *et al.*, 2010; Vogel *et al.*, 2010; Dor *et al.*, 2011; Kohlen *et al.*, 2012, 2013). Therefore, additional enzymes must be involved that give rise to this diversity of SLs in tomato.

Most genes encoding the SL upstream biosynthetic and signalling pathway were elucidated by identifying increased branching mutants using forward genetic approaches (Brewer *et al.*, 2016). A mutation in the recently identified tomato SL biosynthetic gene, *CYP722*, did not cause a more branched phenotype (Wakabayashi *et al.*, 2019), making it impossible to use a forward genetics approach for the remaining unknown SL diversification genes downstream of that gene as they are also not expected to have a branched phenotype.

A common feature of SL biosynthesis genes is that their expression is induced by both phosphate (P) starvation and GR24 application (López-Ráez *et al.*, 2008; Wakabayashi *et al.*, 2019) and we postulated that under such conditions unknown tomato SL biosynthetic genes are co-expressed with the known genes. In this study, a transcriptome analysis of tomato roots grown under those conditions was performed and SL biosynthetic gene candidates identified using co-expression analysis. Using heterologous expression in *Nicotiana benthamiana* and yeast we show that one of these candidates, cytochrome P450 CYP712G1, catalyses the conversion of orobanchol into three DDH isomers, and using systemic virus-induced gene silencing (VIGS), that one of these DDH isomers is an intermediate *en route* to the biosynthesis of solanacol, one of the most abundant SLs in tomato root exudate.

Materials and Methods

Plant growing conditions

For SL analysis, pregerminated seeds of tomato (*S. lycopersicum* cv Moneymaker) were transferred to pots containing a mixture of expanded clay and sand (3 : 1) and grown in the glasshouse at 24°C under a 16 h : 8 h photoperiod using half-strength

© 2022 The Authors
New Phytologist © 2022 New Phytologist Foundation.

Hoagland solution for 2 wk followed by 1 wk continuous half-strength Hoagland solution with P (YP) or without P (NP), as described previously (López-Ráez *et al.*, 2008; Zhang *et al.*, 2018). Root exudate was collected by flushing the pot with 1 l Hoagland solution, which was filtered using filter paper.

Strigolactones were also analysed in tomato grown in aeroponics. Germinated Moneymaker seeds were transferred to rockwool in six 4-cm net cups placed in holes in the lid of an aeroponics bucket. The bucket contained 3 l half-strength Hoagland solution that was sprayed over the roots of the plants every 15 min for 15 s. The plants were grown at 24°C under a 16 h : 8 h photoperiod. After 2 wk, the nutrient solution was replaced using half-strength Hoagland solution with phosphate (YP) or without phosphate (NP). After an additional week, the root exudates (600 ml of the remaining nutrient solution) were collected and processed.

RNA-seq and co-expression analysis

RNA-seq analysis on tomato roots was performed as previously described (Wang *et al.*, 2021) with the addition of a 1 d GR24 application treatment in combination with P deficiency (Supporting Information Fig. S1). RNA isolation and library preparation were performed as described before (Wang *et al.*, 2021).

Pearson correlation coefficients (PCC) were calculated between every two genes in all samples. Comparative Co-Expression Network Construction and Visualization (CoExpNetViz) (Tzfadia *et al.*, 2015) was used to visualise the co-expression network with known SL biosynthetic genes (*SlD27*, *SlCCD7*, *SlCCD8* and *SlMAX1*) as baits and reads per kilobase of transcript, per million mapped reads (RPKM) values of all genes in the RNA-seq dataset as the expression value. The default settings for correlation threshold were used (lower percentile rank < 5; upper percentile rank > 95) and Plaza families (monocots and dicots) (https://bioinformatics.psb.ugent.be/plaza/) were chosen. The co-expression network was displayed using Cytoscape (v.3.5.1) with CoExpNetViz as selected style and group attributes according to colour as layout.

Plasmid construction

The coding sequence (CDS) of tomato CYP712G1 (Solyc10g018150.2) was obtained from SGN (Sol Genomics Network: https://solgenomics.net) (Table S1). The full-length cDNA was amplified from tomato (*S. lycopersicum* L. cv Craigella) root cDNA using primers with restriction enzyme sites included (Table S2). Cloning for agroinfiltration was conducted as previously described (Zhang *et al.*, 2014).

Tobacco rattle virus (TRV)-based vectors TRV1 (Liu *et al.*, 2002) and TRV2B (p1397, GenBank Accession OM677764; TRV RNA2 binary plasmid carrying the 2b gene (Valentine *et al.*, 2004) from TRV isolate PpK20 and a Gateway cassette in reverse-complement orientation for expression of antisense VIGS sequences) were used for VIGS. To generate the inserts, partial fragments of *CYP712G1* and *SlCCD8* (576 bp for *CYP712G1*, 241 bp for *SlCCD8*) were PCR amplified from tomato root cDNA, and the GUS fragment (393 bp) was amplified from pKG1662 using Phusion polymerase (Thermo Fisher Scientific, Vilnius, Lithuania) using primers shown in Table S2. Fragments were inserted into a pDONR207 entry vector using the BP reaction (Thermo Fisher Scientific) and transferred into the TRV2B destination vector using the LR reaction. Finally, the TRV2B VIGS plasmids were transformed into *Agrobacterium tumefaciens* GV3101.

For yeast expression, the gene fragment was amplified from pBIN-Plus-CYP712G1 with the corresponding primers (Table S2). For site-directed mutagenesis, two single mutations p.CYP712G1-D305A, p.CYP712G1-D312A and a double mutation p.CYP712G1-D305A-D312A were generated using primers listed in Table S2. Digestion and ligation were performed to clone CYP712G1, p.CYP712G1-D305A, p.CYP712G1-D312A and p.CYP712G1-D305A-D312A into pYeDP60 into the restriction sites *Not*I and *Pac*I (Pompon *et al.*, 1996; Cankar *et al.*, 2011). The resulting plasmids were transformed into *Saccharomyces cerevisiae* strain WAT11 (Pompon *et al.*, 1996).

Nicotiana benthamiana transient expression

For transient expression, 4-wk-old *N. benthamiana* plants were used for agroinfiltration. The preparation of the *A. tumefaciens* AGL0 strains ($OD_{600} = 0.5$) was performed as previously described (Zhang *et al.*, 2014). A mixture of the CL pathway clones (*SlD27*+ *SlCCD7*+ *SlCCD8*) combined with two rice *MAX1s* (Os900, Os1400) was co-infiltrated to reconstitute the orobanchol pathway in *N. benthamiana*. The mixing of combinations and injection of the bacterial suspension into the leaves were performed as described before (Zhang *et al.*, 2018). After 6 d, the infiltrated leaves were harvested and frozen until further analysis. Six biological replicates were used for each combination.

Virus-induced gene silencing in tomato

Tomato plants were grown as described above using half-strength Hoagland solution for watering. For agroinfiltration, GV3101 cultures containing TRV1 and TRV2 were harvested by centrifugation, resuspended in induction medium (containing 0.5% MS basal medium, 10 mM 2-(*N*-morpholino)ethanesulfonic acid (MES) pH 5.6, 20 g l^{-1} sucrose and 200 μM acetosyringone) to a final OD600 of 1 and mixed at room temperature for 2 h. The bacterial suspension was infiltrated into the abaxial side of the cotyledons of 9-d-old tomato seedlings using a syringe without a needle. Root exudates and root material were collected 28 d after infiltration. Roots were frozen in liquid nitrogen and stored at −80°C for qPCR. At 1 wk before harvest, the nutrient solution was changed into half-strength Hoagland without phosphate.

Gene expression analysis

Total RNA was extracted with TRIzol (Invitrogen) and 800 ng was converted to cDNA using oligo-dT18 primers, dNTPs and RevertAid Reverse Transcriptase (Thermo Fisher Scientific).

© 2022 The Authors
New Phytologist © 2022 New Phytologist Foundation.

Q-PCR was performed on a 7300 Real-Time PCR System (Applied Biosystems, Foster City, CA, USA). The relative gene expression was determined using the comparative threshold cycle value. Tomato reference genes were selected as previously described (Zhang *et al.*, 2018; Wang *et al.*, 2021). Primers used for RT-qPCR are shown in Table S2. To compare gene expression in TRV2B-SlCCD8 and TRV2B-SlCYP712G1 VIGSed plants, the expression levels were normalised to the expression levels in the TRV2B-GUS control plants. Five to six biological replicates were used per treatment.

Yeast microsome *in vitro* assay

Wild-type yeast WAT11 was cultured in YPGA medium and transformed yeast was maintained in SGI medium (Zhang *et al.*, 2014). Induction of gene expression and isolation of microsomes was done as described (Pompon *et al.*, 1996; Zhang *et al.*, 2014) The concentration of the isolated microsomes was determined using the Bicinchoninic Acid protein assay (Sigma).

For yeast microsome *in vitro* assays, orobanchol was incubated with 100 µl (2000 µg protein ml^{-1}) of microsomal protein preparation in a 500 µl reaction containing 1 mM NADPH and 40 mM phosphate buffer (pH = 7.5) in a 1.5 ml Eppendorf vial. The assays were carefully agitated at a moderate speed (200 rpm) for 3 h at 30°C. The reaction was stopped by adding 1.5 ml ethyl acetate.

SL extraction and sample preparation

For SL extraction from *N. benthamiana* leaves (200 mg frozen ground material) and the yeast microsome assay, ethyl acetate was used. SL analysis followed reported methods (Kohlen *et al.*, 2011), but GR24 was used as an internal standard. SL extracts in a mixture of ethyl acetate (50 µl) and 4 ml *n*-hexane were applied to a Strata® SI-1 Silica (200 mg/3 ml) column, preconditioned with 2 ml of ethyl acetate and 4 ml of hexane. The column was washed with *n*-hexane and eluted with 3 ml of 10 : 90 hexane : ethyl acetate. The solvent was evaporated under vacuum, and the residue reconstituted in 100 µl acetonitrile : water (1 : 4) and filtered with Micro Spin (centrifuge) filters 0.2NY (Thermo Fisher Scientific, Waltham, MA, USA) before analysis using multiple reaction monitoring (MRM)-LC–MS/MS.

For collection of root exudate from VIGS-treated plants, root exudates were concentrated using solid phase extraction (SPE) C18 columns (500 mg/6 ml; Sigma-Aldrich) following the method described above. Here, 10 µl of 5×10^{-7} µmol $µl^{-1}$ GR24 standard was added to the eluent, then samples were evaporated to dryness. The residue was reconstituted in ethyl acetate (50 µl) and hexane (4 ml) and purified using SPE, and prepared for LC–MS/MS analysis, as described above.

Detection and quantification of strigolactones using UHPLC–MS/MS

Ultrahigh performance liquid chromatography tandem mass spectrometry (UHPLC–MS/MS) analysis of orobanchol (isomers), solanacol, DDH isomers and hydroxy-orobanchol in *N. benthamiana* leaf extracts, root exudates of tomato and yeast assay extracts was carried out using an Acquity UPLC® system (Waters, Milford, MA, USA) coupled to a Xevo® TQ-XS triple–quadrupole mass spectrometer (Waters MS Technologies, Manchester, UK) with the electrospray interface. Here, 5 µl were injected on a reverse-phase Acquity UPLC™ BEH C18 column (2.1 × 100 mm, 1.7 µm; Waters) at 45°C and separated by applying a water and acetonitrile gradient with 0.1% formic acid as the eluent additive at a flow rate of 0.45 ml min^{-1}. The gradient started from 10% acetonitrile for 2 min, was raised to 50% acetonitrile in 6 min, followed by a gradient to 65% acetonitrile in 1 min and subsequently increased to 95% in 1.5 min, which was maintained for 1 min before going back to 15% acetonitrile using a 0.5 min gradient, and maintained for 2.5 min to equilibrate the column before the next run. The mass spectrometer was operated in positive electrospray ionisation mode with the conditions: capillary voltage (1.2 kV), ion source/desolvation temperature (120/550°C), desolvation/cone gas flow (1000/150 l h^{-1}), cone voltage (15–36 V) and collision energy (10–25 eV). the instrument operation and data analysis were performed using MassLynx™ software (v.4.2; Waters).

To improve separation of DDH isomers an enantio-selective column (Lux™ Cellulose-1, 3 × 150 mm, 3 µm; Phenomenex, Torrance, CA, USA) was used that was eluted using a 28 min gradient of 0.1% formic acid in methanol : water (1 : 9, v/v, A) and 0.1% formic acid in acetonitrile (B) at a flow rate 0.25 ml min^{-1}. The column temperature was maintained at 45°C. The linear binary gradient was set as follows: isocratic elution at 15% B for 1.5 min, linear increase to 27% B in 2.5 min, to 40% B in 6 min and 65% B in 7 min; isocratic elution for 2 min at 65% B, followed by a column wash at 95% B for 4 min and column equilibration to initial conditions. The eluate was introduced into the electrospray ion source of the LC–MS/MS, operating at above-mentioned conditions. DDH isomer naming was synchronised with Zhang *et al.* (2018) using the order of elution (on C18) and the ratio between the MRM channels used that is distinct for the three isomers detected.

Phylogenetic analysis

To construct a phylogenetic relationship for the *CYP712* gene family, homologous protein sequences were mined from genome assemblies of 14 species across the flowering plants (Dataset S1) and new transcriptomes from tobacco roots (Short Read Archive (SRA) accession number SRR7540357), *Astragalus sinicus* (SRA accession number SRR13286078) and *Cosmos bipinnatus* (SRA accession number SRR3546768-9) were assembled *de novo* using the Trinity pipeline (Grabherr *et al.*, 2011; Qin *et al.*, 2020). We also included available sequences from *Bupleurum chinense* and *Aralia elata* (Araliaceae) as representatives of the Apiales order and the putative friedelin C-29 oxidase sequence from *Maytenus ilicifolius* (Sui *et al.*, 2011; Bicalho *et al.*, 2019; Cheng *et al.*, 2020). Some genes of *Kingdonia uniflora* (KAF6168288), *Nyssa sinensis* (KAA8520263) and *Trifolium pratense* (Tp57577_TGAC_v2_mRNA4964) were manually re-annotated based on homology with other known

© 2022 The Authors
New Phytologist © 2022 New Phytologist Foundation.

CYP712 genes. Multiple sequence alignment was performed with MAFFT v.7.450 with automatic selection of appropriate algorithm, BLOSUM62 scoring matrix, a gap open penalty of 1.26 and an offset value 0.123 (Katoh & Standley, 2013) The optimal model of protein sequence evolution for the alignment (CPREV+I+G) was estimated based on second order Akaike information criterion (AICc) using MODELTEST-NG v.0.1.7 (Darriba *et al.*, 2019). The gene tree was reconstructed in a Bayesian framework using MRBAYES v.3.2.6 (Ronquist & Huelsenbeck, 2003) implemented in GENEIOUS PRIME with two independent runs each with a chain length of 2.2 million generations; sampling every 1000th generation; four heated chains with a temperature of 0.2 and applying the optimal model of sequence evolution. CYP93A3 subfamily sequences from the basal angiosperm *Amborella trichopoda* were used as the outgroup. After discarding the first 220 000 generations as burn-in all effective sampling sizes per run were at least 339, the standard deviation of clade frequencies was below 0.007 and the potential scale reduction factor (PSRF) was 1.000, suggesting appropriate convergence between the two runs.

Protein modelling and substrate docking

Homology models were constructed for the tomato CYP712G1, a *Medicago* homologue and two homologues from tobacco (short and long) using CYP76AH1 from *Salvia miltiorrhiza* (PDB ID: 5YLW) and CINNAMATE 4-HYDROXYLASE (C4H1) from *Sorghum bicolor* (PDB ID: 6VBY) as templates, using MODELLER v.9.22 (Webb & Sali, 2016). The sequence identities with CYP76AH1 are 32.8, 30.2, 32.8% and 32.8% and with C4H1 28.7, 28.7, 26.6%, and 26.6% for CYP712G1, the *Medicago* and the two tobacco homologues, respectively. Fig. S2 depicts the alignments of each to the two templates. The heme group present in the CYP76AH1 structure was modelled as a flexible residue. Four orobanchol isomers were used in a docking analysis using AUTODOCK VINA v.1.1.2 (Trott & Olson, 2010). Three residues THR311, ASP312 and THR313 represent the conserved P450 oxygen-binding motif (Werck-Reichhart & Feyereisen, 2000). To take this known interaction into account, these three were modelled as flexible residues allowing them to change and influence the docking process. In addition, 6-hydroxy-orobanchol and 7-hydroxy-orobanchol were docked with CYP712G1 with ASP305 also considered as a flexible residue along with the previously described three, as this aspartate is found within the active site and therefore could also play the role of a proton donor.

Results

The discovery of SL biosynthesis candidate genes

P starvation of tomato resulted in a strongly increased production of orobanchol, solanacol and DDH isomers in both aeroponics (Fig. S3a–c) and in pots with sand/clay (Fig. S3d–f). Upon inspection of our RNA-seq data (Wang *et al.*, 2021), expression of known SL biosynthetic genes (*SlD27*, *SlCCD7*, *SlCCD8* and *SlMAX1*) turned out to be induced by P starvation, repressed by P replenishment and upregulated by GR24 application (under P starvation) (Fig. S4a,b). Furthermore, expression of *SlD27* and *SlCCD7* was induced, whereas expression of *SlMAX1* was repressed in the *CCD8* RNAi line (Fig. S4a,b). Subsequently, we therefore used the RNA-seq results for co-expression analysis using the known SL biosynthetic genes (*SlD27*, *SlCCD7*, *SlCCD8* and *SlMAX1*) as baits. A co-expression network of all

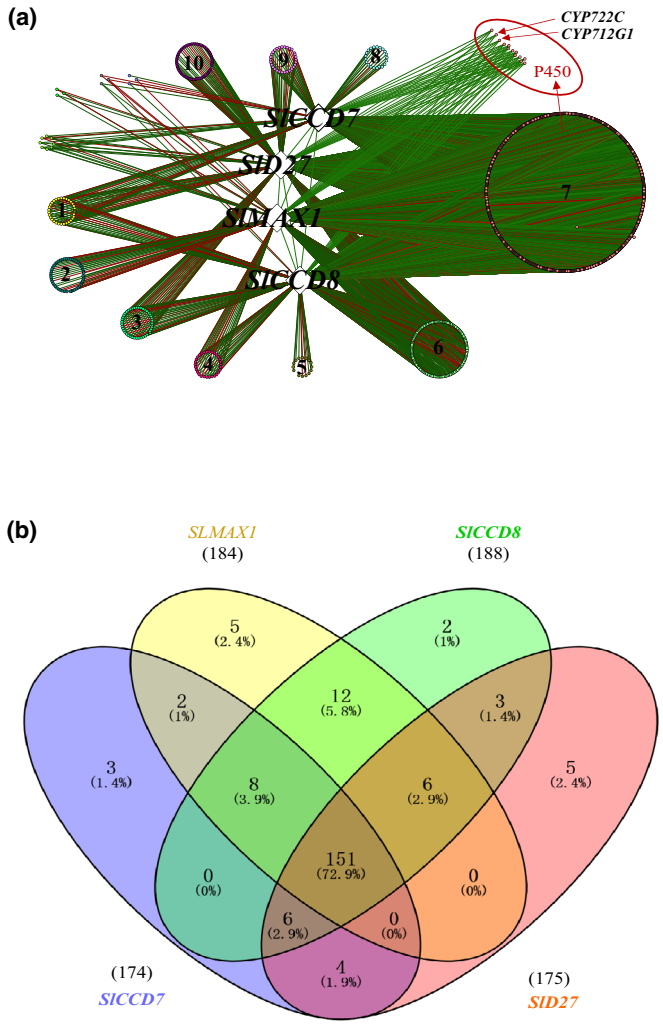

Fig. 2 The discovery of strigolactone (SL) biosynthesis candidate genes in tomato (*Solanum lycopersicum*). (a) Gene co-expression network of all genes in the RNA-seq dataset with four bait genes created with COEXPNETVIZ and CYTOSCAPE. The default correlation threshold of COEXPNETVIZ was used (lower percentile rank < 5; upper percentile rank > 95). Genes in group 1 are co-expressed with *SlD27*, *SlCCD7* and *SlCCD8*; genes in group 2, are co-expressed with SlMAX1; genes in group 3 are co-expressed with *SlD27* and *SlCCD8*; genes in group 4 are co-expressed with *SlCCD8* and *SlMAX1*; genes in group 5 are co-expressed with *SlCCD8*; genes in group 6 are co-expressed with *SlD27*, *SlCCD8* and *SlMAX1*; genes in group 7 are co-expressed with *SlD27*, *SlCCD7*, *SlCCD8* and *SlMAX1*; genes in group 8 are co-expressed with *SlCCD7*; genes in group 9 are co-expressed with *SlD27* and *SlCCD7*; genes in group 10 are co-expressed with SlD27. The 12 P450s we studied in this paper and CYP722C from group 7 were manually moved to a different location on the network canvas (P450 circle on the top right). (b) Venn diagram showing the number of co-expressed genes with known SL biosynthetic genes (PCC ≥ 0.9) (Oliveros, 2007).

© 2022 The Authors
New Phytologist © 2022 New Phytologist Foundation.

the genes in the RNA-seq dataset showed that the genes clustered into 10 differently co-expressed groups (Fig. 2a) and we decided to focus on the genes in group 7 that are co-expressed with all four bait genes. In earlier research, we hypothesised that cytochrome P450s play a role in the conversion of orobanchol into other SLs in tomato (Zhang *et al.*, 2018) and therefore we focused on the P450s in our candidate gene list (Fig. 2a). Among these is the recently published SlCYP722C (Wakabayashi *et al.*, 2019) (Fig. 2a) with a PCC value with all the four bait genes between 0.85–0.9 (Table S3).

CYP712G1 converts orobanchol into DDH in *N. benthamiana*

We successfully cloned 10 out of 12 of the P450s with a PCC of > 0.9 (Fig. 2b; Table S3). To characterise these candidate genes, we transiently co-expressed each of them with the orobanchol-producing biosynthetic pathway in *N. benthamiana*. Since at the time of these experiments, CYP722C had not been published, we co-expressed two *MAX1*s from rice (*Os900* and *Os1400*) with the tomato CL pathway (*SlD27*, *SlCCD7* and *SlCCD8*) to generate orobanchol. This indeed resulted in the production of orobanchol in *N. benthamiana* (Figs 3a, S5). Of the 10 tomato P450 genes, only co-expression of P450.3 (*CYP712G1*) with the five orobanchol pathway genes resulted in significant consumption of orobanchol (Figs 3a, S5a). At the same time, on an enantio-selective column, three peaks of DDH isomers appeared (Fig. 3b). This matches the pattern of DDH isomers in the root exudate of tomato as obtained from the aeroponics system (Fig. 3d). Intriguingly, also a trace amount of solanacol was produced (Fig. 3c). We assumed that this minor conversion was due to a *N. benthamiana* enzyme that can convert DDH into solanacol (please refer to the following sections). These results make CYP712G1 a very likely candidate for SL biosynthesis in tomato. Indeed, in our RNA-seq dataset, the expression pattern of *CYP712G1* (Fig. S4c) was very similar to that of the known SL biosynthetic genes (Fig. S4a,b).

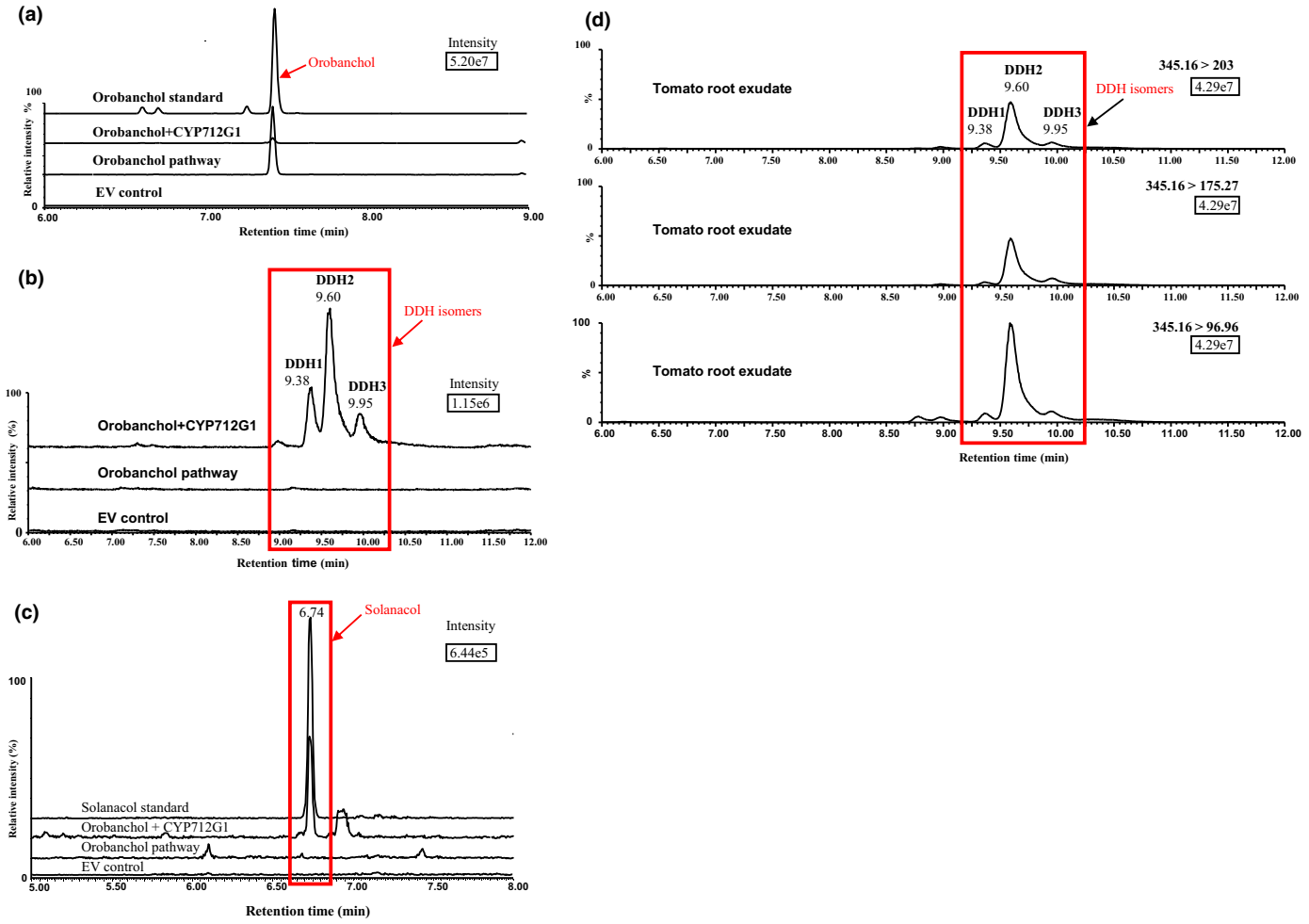

Fig. 3 Biochemical characterisation of *CYP712G1* using transient expression in *Nicotiana benthamiana*. (a) The reduction of orobanchol (transition $[M+H]^+$ *m/z* orobanchol_347.2 > 97) in the transient expression assay. (b) The multiple reaction monitoring (MRM) chromatogram of didehydro-orobanchol (DDH) isomers (transition $[M+H]^+$ *m/z* 345.16 > 96.96) on enantio-selective column in transient expression assay. (c) The production of solanacol (transition $[M+H]^+$ *m/z* 343.16 > 96.97) in the transient expression assay. (d) The MRM chromatogram of DDH isomers (transition $[M+H]^+$ *m/z* 345.16 > 96.96, 345.16 > 175.27 and 345.16 > 203) on enantio-selective column in tomato root exudate under aeroponic system. EV, empty vector; orobanchol pathway, *SlD27* + *SlCCD7* + *SlCCD8* + *Os900* + *Os1400*; orobanchol + CYP712G1, co-expression of *CYP712G1* with the orobanchol pathway.

© 2022 The Authors
New Phytologist © 2022 New Phytologist Foundation.

Orobanchol accumulates when CYP712G1 is silenced

To characterise the function of CYP712G1 *in planta*, we silenced *CYP712G1* in tomato plants using VIGS and measured the production of SLs in the root exudate. GUS was used as a negative control and the SL biosynthetic gene *SlCCD8* as a positive control. Quantitative RT-PCR showed a 29% nonsignificant decrease in the expression of *SlCCD8* in the root of TRV2B-SlCCD8 plants compared with the control (TRV2B-GUS) (Fig. 4a). Interestingly, the expression of *SlCCD7*, *SlMAX1* and SlCYP712G1 increased 3.98-, 1.39- and 2.13-fold, respectively, compared with the TRV2B-GUS control, probably due to feedback upregulation. Unexpectedly, the expression of *SlD27* decreased by 31% (Fig. 4a), possibly as a result of its presence at the branch point of both ABA and SL biosynthesis (Abuauf *et al.*, 2018). Compared with the control (TRV2B-GUS), the amounts of orobanchol, solanacol and DDH isomers in the root exudate of tomato plants with silenced *SlCCD8* were strongly reduced (Fig. 4b–d), showing that VIGS can, systemically, alter SL biosynthesis in the roots of tomato, as reported before (Xu *et al.*, 2018) and that this also results in decreased SL levels in the root exudate. The combination of a strong reduction in SLs while gene expression was not significantly affected is likely to be due to the experimental system, as silencing efficiency may be patchy, the root system can only be retrieved partially, and root exudates are collected from the entire root system.

RT-PCR showed that VIGS reduced the expression of *CYP712G1* (nonsignificantly) by 12% compared with the control (TRV2B-GUS) (Fig. 4a). The expression of *SlD27* decreased – just as in the *SlCCD8*-silenced plants – while the expression of the other SL biosynthetic genes, *SlCCD7*, *SlCCD8* and *SlMAX1*, increased – similar as occurred in the *SlCCD8*-silenced plants (Fig. 4a). Together, the changes in gene expression upon silencing of *CYP712G1* closely resembled the effect seen when silencing *CCD8*. VIGS of *CYP712G1* resulted in a 12.2-fold higher concentration of orobanchol compared with the TRV2B-GUS-treated plants (Fig. 4b) supporting the assumption that the encoded enzyme uses orobanchol as substrate. Furthermore, the amount of DDH and solanacol decreased, although only by 10.9% and 26.2%, respectively, with the former not being statistically significant (Fig. 4c,d). The larger orobanchol increase (compared with the decrease in DDH and solanacol) is possibly caused by the feedback upregulation of upstream genes resulting in higher orobanchol production in the *SlCYP712G1* silenced plants (Fig. 4a). The accumulation of orobanchol and the decrease in DDH and solanacol supported the assumption that solanacol is derived from orobanchol by one or more of the DDH isomers and that CYP712G1 is the tomato SL biosynthetic enzyme that catalyses these reactions.

CYP712G1 catalyses the conversion of orobanchol into DDH

To further confirm the function of CYP712G1, we expressed *CYP712G1* in the yeast strain WAT11 (Pompon *et al.*, 1996) and incubated isolated microsomes with orobanchol. MRM-LC/MS/MS analysis showed the formation from orobanchol of two DDH isomers (Fig. S6). No further conversion to solanacol was observed (data not shown). To obtain a better separation of the DDH isomers, we used an enantio-selective column and this allowed us to detect three DDH isomers just as in *N. benthamiana* and tomato root exudate, albeit at different ratios (Fig. 5). This confirms that CYP712G1 catalyses the conversion of orobanchol into DDH isomers with DDH3 being the dominant product in the yeast microsome assay.

To test if CYP712G1 displayed substrate stereo-selectivity, we assessed the enzymatic efficiency of the microsomes expressing CYP712G1 with all four orobanchol stereoisomers (Fig. 5a). MRM-LC/MS/MS analysis revealed that CYP712G1 can also catalyse the conversion of 2′-*epi*-orobanchol into DDH isomers although with substantially lower efficiency compared with orobanchol (Figs 5b, S6). On the enantio-selective column, these 2′-*epi*-orobanchol-derived DDH isomers (DDHa, b, c) eluted later compared with the DDH isomers naturally occurring in root exudate of tomato and produced in transient expression in *N. benthamiana* (Figs 5b, S6).

CYP712G1 produces hydroxy-orobanchol as an intermediate *en route* to DDH

In addition to the formation of DDH isomers, also two hydroxy-orobanchol-like compounds were produced from both orobanchol and 2′-*epi*-orobancol in the yeast assay (Fig. S7). This putative identification is based on the comparison with a standard of the tentatively identified 7-hydroxy-orobanchol that has previously been reported to be present in root exudate of tomato and cucumber (Kohlen *et al.*, 2013; Khetkam *et al.*, 2014). The 7-position in this hydroxy-orobanchol has however not been unambiguously proven (Khetkam *et al.*, 2014). The presence of two peaks could therefore represent the production of stereoisomers of 7-hydroxy-orobanchol and/or the production of a C5 and/or C6-hydroxy-orobanchol (in addition to C7), which theoretically could all serve as intermediates in the formation of solanacol (Fig. S8). The use of shorter incubation times showed that the enzyme is active for several hours, but did not result in changes in the ratio between hydroxy-orobanchol and DDH (Fig. S9). After 24 h of incubation with orobanchol, most of the DDH had been decomposed (Fig. S9a). This suggests the instability of DDH (K. Yoneyama & X. Xie, pers. comm.) and is also the reason why we were unable to isolate sufficient DDH for structure elucidation.

Modelling CYP712G1 structure and substrate docking

To further underpin the mechanism – and substrate- and regio-specificity – of the CYP712G1 catalysed conversion of orobanchol to DDH, we created a structural model of the enzyme using homology modelling. The CYP712G1 protein model with the heme group (Fig. S10a) exhibited a normalised DOPE score of −0.89, which was close to the 'near-native' score of −1 and represents a good model (Eramian *et al.*, 2008). Docking analysis of this model with the four orobanchol isomers (Fig. 6a–d) showed that CYP712G1 docks orobancol and 2′-*epi*-orobanchol in an orientation allowing for the subsequent hydroxylation reaction

© 2022 The Authors
New Phytologist © 2022 New Phytologist Foundation.

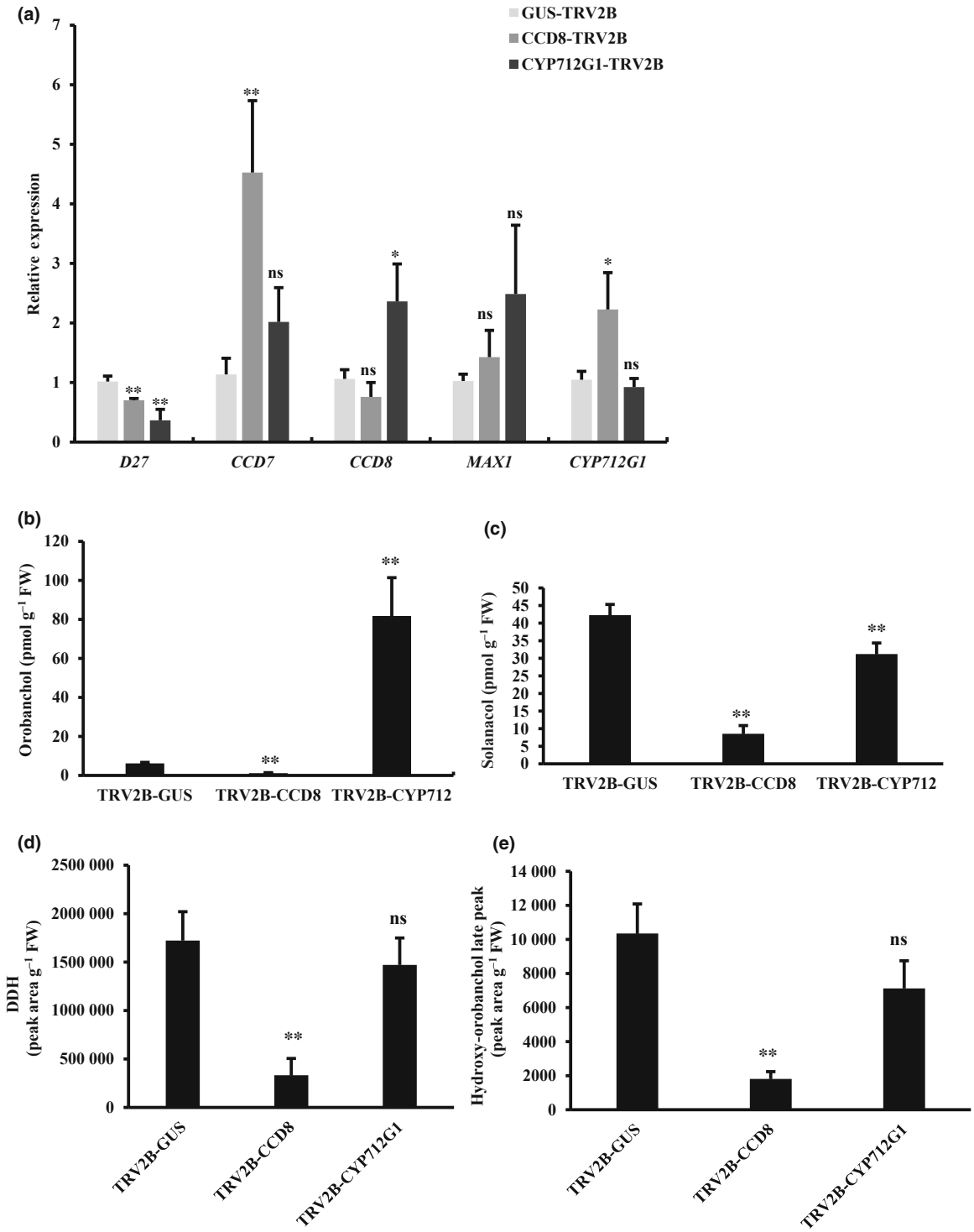

Fig. 4 Expression of strigolactone (SL) biosynthetic genes in roots and SL quantification in the root exudate of virus-induced gene silencing (VIGS)-treated tomato plants (cv Moneymaker). (a) The expression of *D27*, *CCD8*, *MAX1* and *CYP712G1*, normalised to two reference genes (*SGN-U584254* and *SGN-U563892*; Dekkers *et al*., 2012), in the roots of tomato (cv Moneymaker) 4 wk after infiltration of leaves with tobacco rattle virus (TRV) VIGS constructs ($n = 6$). (b) Orobanchol level (transition $[M+H]^+$ *m/z* orobanchol_347.2 > 97) in the root exudate of VIGS-treated tomato plants. (c) Solanacol level (transition $[M+H]^+$ *m/z* solanacol_343.16 > 96.97) in the root exudate of VIGS-treated tomato plants. (d) DDH isomers level (transition $[M+H]^+$ *m/z* DDH_345.16 > 96.96) in the root exudate of VIGS-treated tomato plants. (e) Hydroxy-orobanchol level (transition $[M+H]^+$ *m/z* hydroxy-orobanchol_361.16 > 247.05) in the root exudate of VIGS-treated tomato plants. Root exudates were collected after VIGS infiltration for 4 wk (normalised using root fresh weight, pmol g^{-1} FW), GUS-TRV2B is the experimental control and CCD8-TRV2B is the positive control ($n = 6$). Error bars represent means ± SEM (significance was determined using Student's *t*-test, * and ** = significant at 0.05 and 0.01 levels, respectively; ns, nonsignificant).

© 2022 The Authors
New Phytologist © 2022 New Phytologist Foundation.

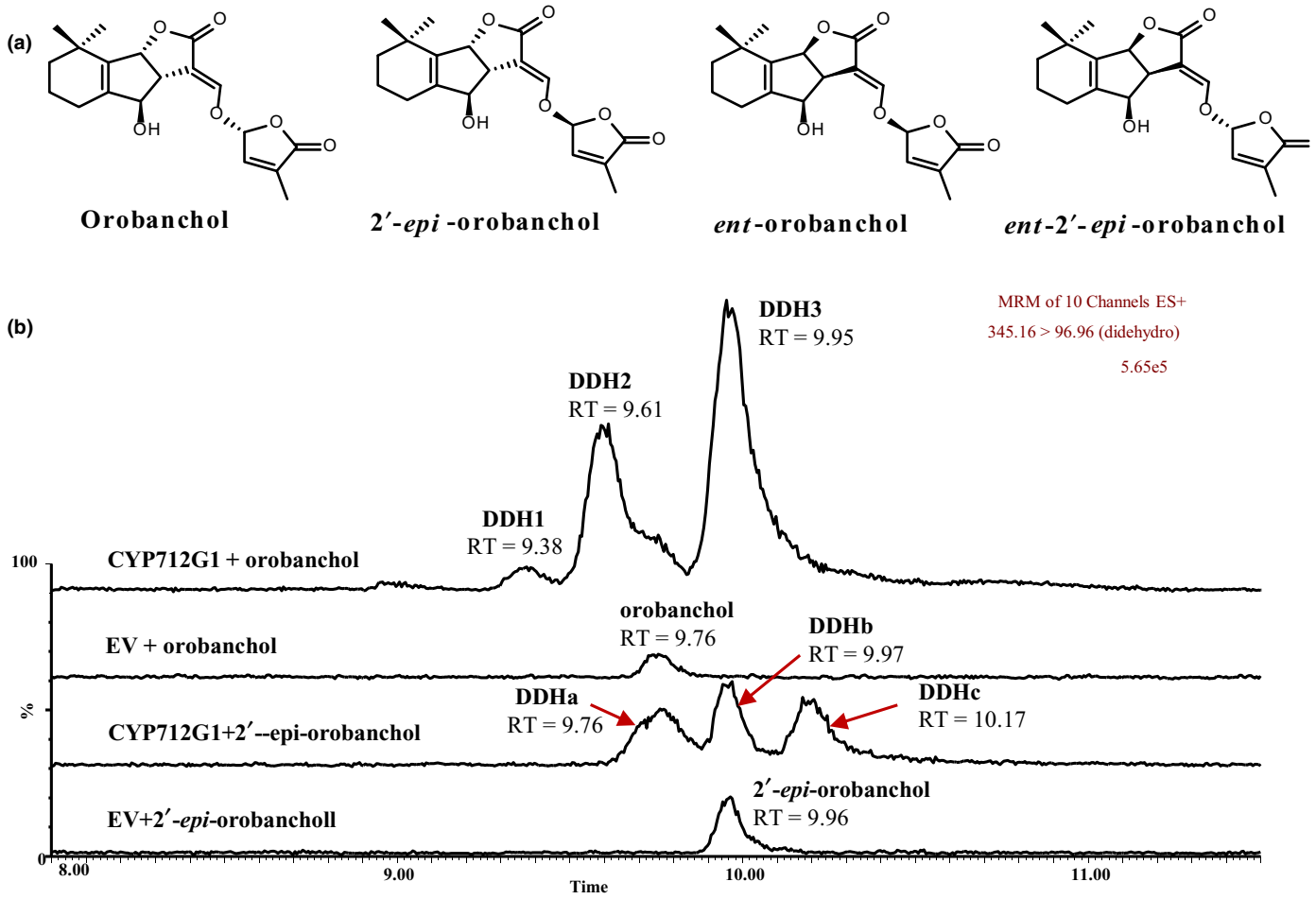

Fig. 5 Multiple reaction monitoring-liquid chromatography tandem mass spectrometry (MRM-LC/MS/MS) identification of didehydro-orobanchol (DDH) isomers and orobanchol stereoisomers of yeast microsome *in vitro* assay on enantio-selective column. (a) Structures of orobanchol stereoisomers. (b) Representative chromatogram of the production of DDH isomers (transition $[M+H]^+$ *m/z* DDH_345.16 > 96.96) in the enzyme assay mixture with yeast microsomes expressing *CYP712G1* (empty vector (EV) as control) and two orobanchol isomers after incubation of 3 h as analysed using MRM-LC–MS ($n = 3$) on an enantio-selective column.

to occur (Fig. 6a,b), whereas *ent*-2′-*epi*-orobanchol and *ent*-orobanchol dock (Fig. 6c,d) in a reverse orientation. This supports the result with the yeast assays, showing that CYP712G1 prefers orobanchol and – to a lesser extent – 2′-*epi*-orobanchol as substrates, but not *ent*-2′-*epi*-orobanchol and *ent*-orobanchol.

The docking analysis showed that orobanchol docks into the enzyme with C7 and C6 facing the heme (Fig. 6a; distances to Fe atom in heme 3.5 and 4.2 Å, respectively). This suggests that C7 and C6 are the most likely positions for hydroxylation (path 1 and path 2 in Fig. S8). So that we could speculate that the two hydroxy-orobanchol-like peaks (Fig. S7a) we obtained in the yeast microsome assay of CYP712G1 with orobanchol represent C6- and C7-hydroxy-orobanchol. 2′-*Epi*-orobanchol docks with C7 facing the heme (4.7 Å; Fig. 6b) suggesting that the two hydroxy-*epi*-orobanchol-like peaks (Fig. S7a) obtained with *epi*-orobanchol as substrate represent the stereoisomers of C7-hydroxy-*epi*-orobanchol, although it cannot be excluded that they represent C6- and C7-hydroxy-*epi*-orobanchol.

Two aspartic acid residues are indispensable for the activity of CYP712G1

Docking results suggested that two aspartic acids at positions 305 and 312 are located in the vicinity of 6-hydroxy- and 7-hydroxy-orobanchol (Fig. 6e,f) and therefore may be involved in the proton donation required for the conversion (Fig. S8). To test how important these two aspartic acids are in the activity of CYP712G1, protein mutants (p.CYP712G1-D305A, p.CYP712G1-D312A, p.CYP712G1-D305A–D312A) were expressed in yeast and incubated with orobanchol as substrate. MRM-LC/MS/MS analysis showed that p.CYP712G1-D312A still displayed some DDH producing activity (Fig. S11a). However, neither p.CYP712G1-D305A nor p.CYP712G1-D305A–D312A produced any detectable DDH (Fig. S11). The production of hydroxy-orobanchol by these mutants showed the same trend as for DDH (Fig. S11b). These results showed that these two aspartic acids are indeed essential for the enzymatic activity of CYP712G1.

© 2022 The Authors
New Phytologist © 2022 New Phytologist Foundation.

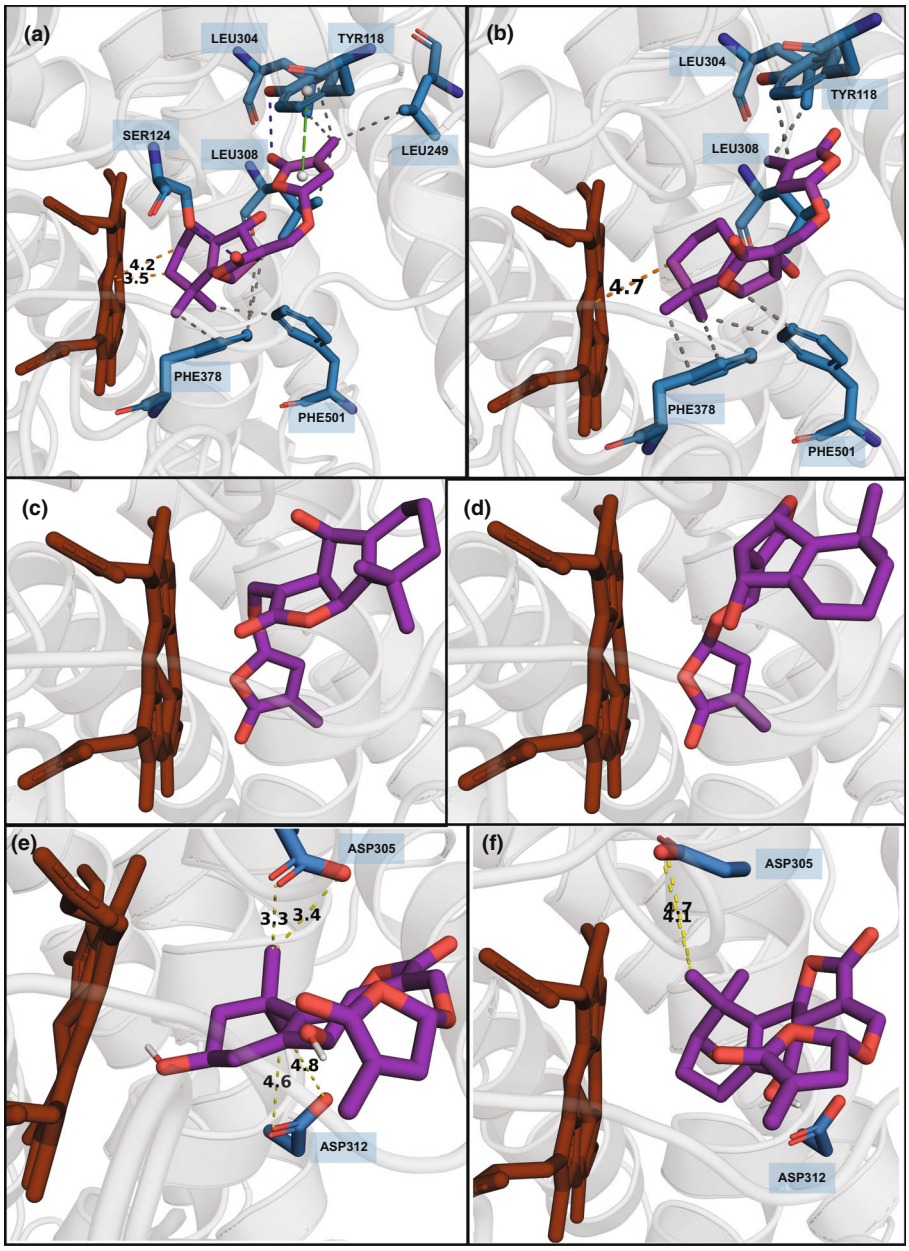

Fig. 6 Docking of potential substrates into tomato CYP712G1. Docking of (a) orobanchol, (b) 2′-*epi*-orobanchol, (c) *ent*-orobanchol, (d) *ent*-2′-*epi*-orobanchol, (e) 6-hydroxy-orobanchol and (f) 7-hydroxy-orobanchol into CYP712G1. All substrates are depicted in purple, the heme in brown and protein residues in blue. The distances (in Å) of C7 and C6 in (a) and C7 in (b) to the Fe group of the heme are shown in orange. Other interactions of (a) and (b) to residues in CYP712G1 as returned by the Protein-Ligand Interaction Profiler (PLIP) tool (Salentin *et al*., 2015) are shown and the residues are labelled – hydrophobic interactions as dashed grey lines, π-Stacking as dashed green lines, and hydrogen bonds as dashed blue lines. Both (a) and (b) are involved in hydrophobic interactions with neighbouring phenylalanines and leucines (PHE378, PHE501, LEU249, LEU308). Orobanchol (a) can also form hydrogen bonds with SER124 and TYR118. This TYR118 is also positioned in a way to be stabilised using a π-stacking interaction between its aromatic ring and that of the orobanchol (represented as a green dashed line between two white spheres at the centres of the aromatic rings). *Ent*-orobanchol and *ent*-2′-*epi*-orobanchol (d, e) dock in reverse orientation. In (e) and (f) distances of the docked ligand to the two aspartic acids that were mutated are shown if < 5 Å. The binding energies of the ligands for the dockings shown in this figure are provided in Supporting Information Dataset S2.

Phylogenetic analysis of the CYP712 gene family

To better understand the evolutionary context of CYP712G1 in the plant kingdom, a phylogenetic analysis was performed. Homologous protein sequences were retrieved from genome assemblies of species across the core Eudicots such as Rosids and Asterids but also from early-diverging Eudicot orders such as Proteales (*Nelumbo*) and Ranunculales (*Kingdonia*) (Dataset S1), confirming that the gene family originated from a common ancestor of the Eudicot clade (Nelson & Schuler, 2013). This was consistent with DDH having been detected in Eudicots only (Kohlen *et al*., 2013; Xie *et al*., 2013; Tokunaga *et al*., 2015; Xie, 2016). Based on our phylogenetic tree reconstruction, the CYP712 family comprised two main clades (Figs 7, S12). Both

© 2022 The Authors
New Phytologist © 2022 New Phytologist Foundation.

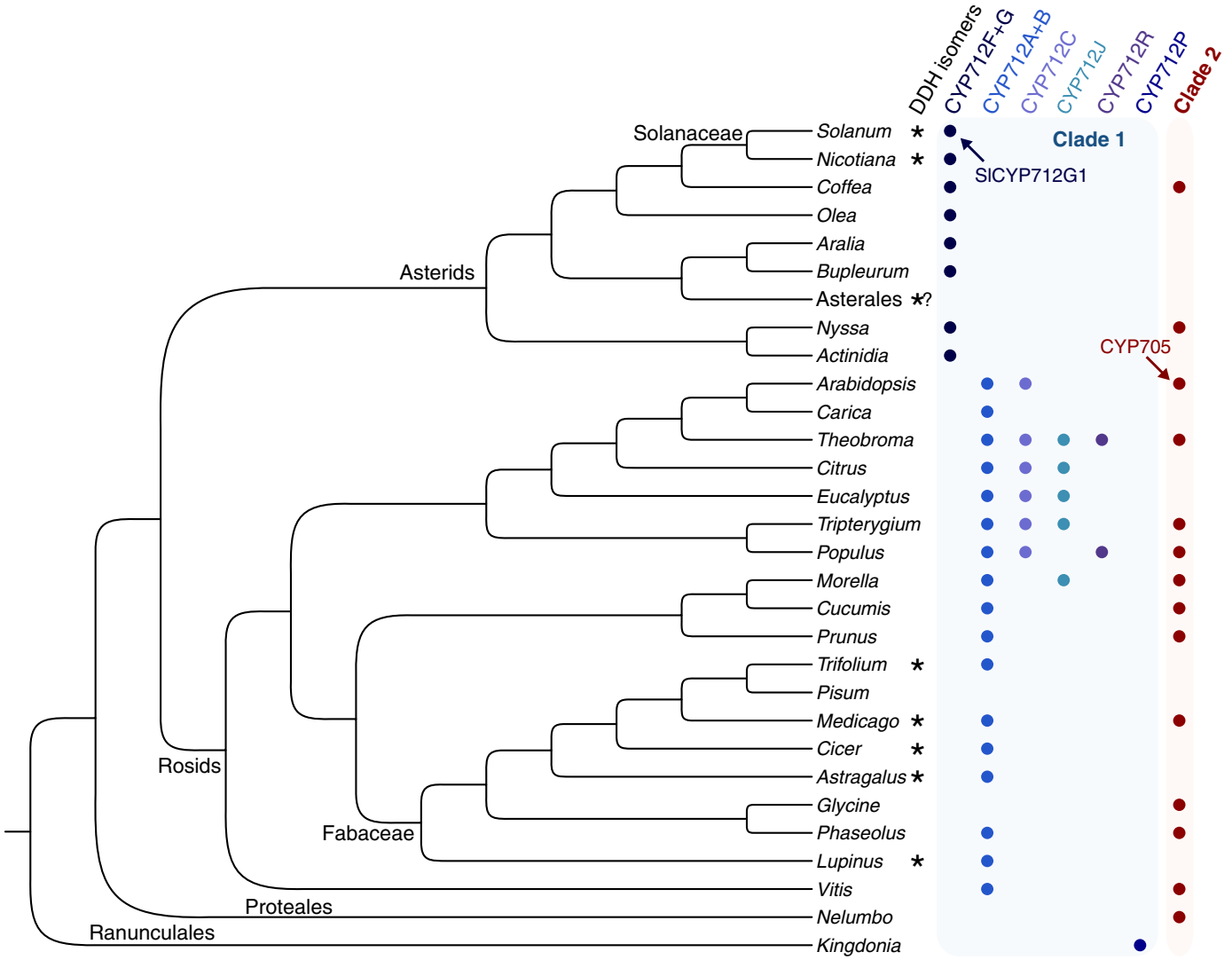

Fig. 7 Distribution of the *CYP712* gene subfamilies across the Eudicot phylogenetic tree. Asterisks indicate described presence of didehydro-orobanchol (DDH)isomers. The black and red arrows indicate tomato (*Solanum lycopersicum*) CYP712G1 and *Arabidopsis* CYP705 subfamilies, respectively.

clades comprised genes from Asterids and Rosids. Genes from basal Eudicots *Nelumbo* and *Kingdonia* are single-copy and appear as sisters to either of the two main clades, suggesting that the two main clades originated from a gene duplication in a common ancestor of the Eudicots. Within clade 1, genes of Asterids (subfamilies CYP712G, CYP712F and CYP712R; including SlCYP712G1) comprised a single clade, whereas those of Rosids (subfamilies CYP712A, CYP712B, CYP712C, and CYP712J) appeared to comprise at least three different orthogroups (Figs 7, S12). Main clade 2 comprises subfamilies CYP712D, CYP712E, CYP712K, and the Brassicales-specific family CYP705 that originated from within the CYP712 family and seems to represent a single orthogroup with lineage-specific duplications (including the large CYP705 family in Arabidopsis) (Figs 7, S12).

The CYP712 family is considered to be derived from a tandem duplication of CYP93 as they share the same intron/exon organisation and are often located adjacent in the plant genome (Fig. S12) (Nelson & Werck-Reichhart, 2011; Du *et al.*, 2016). Members of the CYP93 family are generally involved in flavonoid and triterpenoid biosynthesis (Du *et al.*, 2016). Genes reported to be involved in triterpenoid metabolic pathways belong to clade 2, such as thalandiol desaturase (CYP705A5) and an arabidiol cleavage enzyme (CYP705A1) from Arabidopsis and friedelin oxidases from *Tripterygium* and *Maytenus* (CYP712K1–4) (Fig. S12) (Sohrabi *et al.*, 2015; Bicalho *et al.*, 2019; Huang *et al.*, 2019; Hansen *et al.*, 2020). Therefore a likely scenario could be that clade 2 has maintained or further evolved functions in triterpenoid metabolism, whereas clade 1 has evolved new functions in SL biosynthesis.

Discussion

In the present study, using RNA-seq and co-expression analysis and reconstruction of the tomato SL pathway in *N. benthamiana*, we showed that cytochrome P450, CYP712G1, catalyses the conversion of orobanchol into three DDH isomers. Additional *in vivo* (silencing *CYP712G1* with VIGS) and *in vitro* (yeast microsome assay) experiments provide further evidence that

© 2022 The Authors
New Phytologist © 2022 New Phytologist Foundation.

CYP712G1 is an orobanchol oxidase that converts orobanchol into three DDH isomers (Fig. 1). Our study also suggests that one of these DDH isomers, DDH3, is the substrate for solanacol (Fig. 1), which has been proposed in other studies (Rani *et al.*, 2008; Xie *et al.*, 2010; Kohlen *et al.*, 2012; Xie, 2016).

Similarly, it was also proposed that 7-hydroxy-orobanchol is derived from orobanchol (Xie, 2016). In the present study, yeast microsomes expressing *CYP712G1* produced two peaks from orobanchol in the hydroxy-orobanchol channels, suggesting that two hydroxy-orobanchol-like products are formed. Intriguingly, we only detected the earlier eluting peak in the root exudate of tomato and *N. benthamiana* leaves co-infiltrated with CYP712G1 and the orobanchol pathway (Figs S7, S14). Furthermore, in the VIGS assay, silencing of CYP712G1 caused a reduction in this hydroxy-orobanchol peak in the root exudate, confirming that it is produced by CYP712G1, also *in planta* (Fig. S13). Taken together, we hypothesise that only the later peak of hydroxy-orobanchol detected in the yeast microsome assay was converted into other SLs (DDH and solanacol) (Fig. 1) and therefore did not accumulate, whereas the earlier peak seems to be a side reaction product of CYP712G1 that, *in planta*, is not further converted but is exuded. Modelling and docking also supported a role for CYP712G1 in the conversion of orobanchol to DDH isomers probably through hydroxylation at C6 and/or C7 (Figs 6, S8, S10). Whether hydroxy-orobanchol, and which isomer, is an intermediate of CYP712G1 in the conversion of orobanchol to DDH could be confirmed by incubation of *CYP712G1* expressing microsomes with hydroxy-orobanchol standards that are, however, not available.

The involvement of a cytochrome P450 in the conversion of orobanchol to solanacol was already predicted (Zhang *et al.*, 2018). Our study shows that CYP712G1 is only responsible for the first step towards solanacol production and it is likely that another P450, different from CYP712G1 or alternative oxidising enzyme, is involved in the formation of solanacol from DDH (Fig. 1). We tested 10 other P450s, identified by co-expression analysis, using transient co-expression in *N. benthamiana* in combination with the orobanchol pathway genes and *CYP712G1*, but none of these catalysed the conversion of DDH to solanacol (Fig. S5d–f). Interestingly, the transient expression of P450.6 in *N. benthamiana* resulted in nonspecific activity, decreasing the level of all SLs analysed (Fig. S5), possibly due to its function as a carotenoid β-hydroxylase (Stigliani *et al.*, 2011), which would decrease substrate availability for the SL pathway (Matusova *et al.*, 2005). Assessing the catalytic activity of synthetic cDNAs (for the two genes we were not able to clone) and/or screening more co-expressed P450 genes and/or other oxidising enzymes should enable us to find this last missing step in the tomato solanacol biosynthetic pathway.

Virus-induced gene silencing has been demonstrated before to be a suitable tool to reduce transcription of SL biosynthetic genes in tomato roots and reduce the concentration of orobanchol, solanacol and DDH isomers in the roots (Xu *et al.*, 2018). We show here that also the level of SLs in the root exudate of VIGS-treated plants is significantly decreased.

In our *in vitro* assays, both orobanchol and 2′-*epi*-orobanchol were used as a substrate by CYP712G1, with a preference for orobanchol, the natural substrate. As all SLs are synthesised from CL, 2′-*epi*-orobanchol should not occur in tomato, although *ent*-2′-*epi*-orobanchol has been reported in the close relative, tobacco (Xie *et al.*, 2013).

In the present study the same three DDH isomers were detected in tomato root exudate, in *N. benthamiana* upon transient expression, as well as in the yeast microsome assays. The later shows that all three DDH isomers are produced from orobanchol (Fig. 5b).The ratio between the three isomers, however, differed between the two systems (Fig. 3b,d). DDH2 was dominant in tomato root exudate, DDH3 in the yeast assay (Figs 3d, 5b). It seems likely that in tomato DDH3 is preferentially converted into solanacol, which results in the relative accumulation of DDH2 that ends up in the tomato root exudate (Fig. 3d). The biological significance of the exudation of the DDH isomers into the rhizosphere and their biological activity are unknown.

DDH has been reported in the Fabaceae (*Medicago truncatula*, *A. sinicus*, *Cicer arietinum*, *Lupinus albus*, *Pisum sativum*, *T. pratense*), Solanaceae (*S. lycopersicum* and *Nicotiana tabacum* L.) and Asteraceae (*C. bipinnatus* and *Hedypnois rhagodioloides*) (Figs 7, S12) (Yoneyama *et al.*, 2008, 2011, 2013). Putative orthologues of *CYP712G1* are indeed present in nearly all of these species (Dataset S1). Orobanchol, the probable substrate of the enzymes encoded by these *CYP712G1* orthologues has also been reported in many of these species (Yoneyama *et al.*, 2008). A notable exception is the absence of orthologues in genomic or transcriptomic data for *P. sativum* (Fabaceae). This is however in line with a recent study showing the presence of several SLs in pea, but not DDH (Pavan *et al.*, 2016). We could also not retrieve *CYP712* family members from any Asteraceae, including from our newly generated transcriptome assembly from *C. bipinnatus*. Therefore, based on our hypothesis that Clade 1 *CYP712* genes encode DDH synthases, earlier reports of DDH in Asteraceae such as *C. bipinnatus* (Yoneyama *et al.*, 2011) may be due to misidentification or, alternatively, biosynthesis of DDH isomers in Asteraceae may rely on a different gene family. Docking of the *M. truncatula* CYP712B1 model with four orobanchol isomers (Fig. S15a) showed that 2′-*epi*-orobanchol is the preferred substrate, and oriented in quite a different way to orobanchol in tomato CYP712G1, with the C9 and C10 methyl groups facing the heme group. This fits with the biosynthesis mechanism of medicaol as proposed (Tokunaga *et al.*, 2015), except that orobanchol, rather than *epi*-orobanchol is the likely substrate. Modelling and docking the two tobacco CYP712G1 length variants showed that the C7 of 2′-*epi*-orobanchol and *ent*-2′-*epi*-orobanchol face the heme in the short CYP712G1 protein model, whereas the other two isomers do not dock in the expected orientation (Fig. S15b). In the long tobacco CYP712G1 protein model, only the C7 of 2′-*epi*-orobanchol faces the heme, whereas the other three isomers do not dock in the expected orientation (Fig. S15c). This suggests that tobacco CYP712G1 length variants may accept different orobanchol isomers as substrate, just as the tomato orthologue. Interestingly, as discussed

© 2022 The Authors
New Phytologist © 2022 New Phytologist Foundation.

above, *ent*-2′-*epi*-orobanchol has been reported in tobacco (Xie *et al.*, 2013).

Our modelling and docking results suggest a possible involvement of CYP712 in the conversion of orobanchol in tobacco and *M. truncatula* to DDH isomers/solanacol and medicaol (previously also called a DDH isomer), respectively. Assays with these enzymes should show if this is true. The presence of these 'DDH isomers' (and solanacol) in just a part of the plant kingdom is intriguing. Furthermore, DDH isomers are more abundant compared with solanacol in the root exudate. This suggests that they play a role in the rhizosphere as signalling molecules *per se* – possibly in the communication with beneficial microbes as recently shown for orobanchol and the putative methoxy-5-deoxystrigol isomer in rice (Kim *et al.*, 2022) – and are not just mere precursors of solanacol. Isolation and characterisation, as well as studies on the regulation of their production, should show what is the exact biological role of these compounds.

To date, only the structure of medicaol (called DDH isomer until structure elucidation) has been characterised (Tokunaga *et al.*, 2015). Unfortunately, as explained above, the instability of the tomato DDH isomers prevented isolation and/or synthesis, obstructing verification of their structure and biological activity. Our study has now revealed the tomato enzyme that is involved in DDH (and therefore solanacol) biosynthesis. Potentially this will help in the further identification of the structure of the DDH isomers. Both *in vitro* assays with *CYP712G1* expressing yeast microsomes to which orobanchol is supplied and heterologous expression of the orobanchol pathway with *CYP712G1* in *N. benthamiana* could be used as tools to produce increased amounts of these molecules and, thereby, help elucidate their structure. Our findings also will allow us to modify the tomato root exudate SL composition and therefore open up the opportunity to study the biological relevance of the exudation of DDH isomers and solanacol into the rhizosphere. Results of these studies can potentially be applied in breeding for rhizosphere traits in tomato.

Acknowledgements

This work was supported by a China Scholarship Council (CSC) scholarship 201506300065 (to YW), ERC Advanced grant CHEMCOMRHIZO 670211 (to HJB, KF and LD) and Marie Curie fellowship NEMHATCH 793795 (to LD). SM is funded by the Scottish Government Rural and Environment Science and Analytical Services Division (RESAS). pKG1662 vector was kindly provided by Professor Michel A. Haring (Plant Physiology, University of Amsterdam). We thank Koichi Yoneyama and Xionan Xie (Utsonomiya University) for kindly providing the tentatively identified 7-hydroxy-orobanchol, Alain de Mesmaeker (Syngenta, Stein Switzerland) for providing GR24, Professor Binne Zwanenburg (Radboud University Nijmegen, the Netherlands) for providing four orobanchol stereoisomers and Professor Koichi Yoneyama (Center for Bioscience Research and Education, Utsunomiya University, Japan) for providing solanacol standard. We acknowledge Professor David Nelson (UC Riverside, USA) for help with CYP712 gene classification.

Competing interests

None declared.

Author contributions

YW, LD and HJB designed the research. YW, C-YL and AC performed the experiments. JD and A-JDvD conducted the modelling and docking analysis. HGSD and MHM performed the co-expression analysis. KF and AC performed LC–MS/MS analysis. RvV and MES performed the transcriptome assemblies and phylogenetic analysis. SM provided the TRV2B vector and valuable guidance for performing VIGS experiment. YW, JD, RvV, KF, AD, LD and HJB wrote the manuscript. All authors edited and approved the final manuscript.

ORCID

Harro J. Bouwmeester https://orcid.org/0000-0003-0907-2732
Aalt D. J. Dijkvan https://orcid.org/0000-0002-8872-5123
Lemeng Dong https://orcid.org/0000-0002-1435-1907
Kristyna Flokova https://orcid.org/0000-0002-5558-0669
Che-Yang Liao https://orcid.org/0000-0002-9756-3111
Stuart MacFarlane https://orcid.org/0000-0002-6046-4400
Marnix H. Medema https://orcid.org/0000-0002-2191-2821
M. Eric Schranz https://orcid.org/0000-0001-6777-6565
Robin Velzenvan https://orcid.org/0000-0002-6444-7608
Yanting Wang https://orcid.org/0000-0003-1970-4158

Data availability

The raw reads of the RNA-seq data are available in the NCBI SRA under accession nos. PRJNA679261 and PRJNA686071. The cDNA sequence of tomato CYP712G1 and the assembled mRNA transcripts of *A. sinicus* CYP712B10 and two length variants of tobacco CYP712G1 are available in GenBank under the accession nos. MW384608, MZ476867, MZ476868, and MZ476869, respectively. All transcriptome assemblies and phylogenetic datasets can be accessed at the 4TU. ResearchData portal by https://doi.org/10.4121/14891094.

References

Abe S, Sado A, Tanaka K, Kisugi T, Asami K, Ota S, Kim HI, Yoneyama K, Xie X, Ohnishi T *et al.* 2014. Carlactone is converted to carlactonoic acid by MAX1 in *Arabidopsis* and its methyl ester can directly interact with AtD14 *in vitro*. *Proceedings of the National Academy of Sciences, USA* **111**: 18084–18089.

Abuauf H, Haider I, Jia K-P, Ablazov A, Mi J, Blilou I, Al-Babili S. 2018. The *Arabidopsis DWARF27* gene encodes an all-*trans*–/9-*cis*-β-carotene isomerase and is induced by auxin, abscisic acid and phosphate deficiency. *Plant Science* **277**: 33–42.

Akiyama K, Matsuzaki K-i, Hayashi H. 2005. Plant sesquiterpenes induce hyphal branching in arbuscular mycorrhizal fungi. *Nature* **435**: 824–827.

Akiyama K, Ogasawara S, Ito S, Hayashi H. 2010. Structural requirements of strigolactones for hyphal branching in AM fungi. *Plant and Cell Physiology* **51**: 1104–1117.

© 2022 The Authors
New Phytologist © 2022 New Phytologist Foundation.

Alder A, Jamil M, Marzorati M, Bruno M, Vermathen M, Bigler P, Ghisla S, Bouwmeester H, Beyer P, Al-Babili S. 2012. The path from β-carotene to carlactone, a strigolactone-like plant hormone. *Science* **335**: 1348–1351.

Arite T, Iwata H, Ohshima K, Maekawa M, Nakajima M, Kojima M, Sakakibara H, Kyozuka J. 2007. *DWARF10*, an *RMS1*/*MAX4*/*DAD*1 ortholog, controls lateral bud outgrowth in rice. *The Plant Journal* **51**: 1019–1029.

Bicalho KU, Santoni MM, Arendt P, Zanelli CF, Furlan M, Goossens A, Pollier J. 2019. CYP712K4 catalyzes the C-29 oxidation of friedelin in the *Maytenus ilicifolia* quinone methide triterpenoid biosynthesis pathway. *Plant and Cell Physiology* **60**: 2510–2522.

Bouwmeester H, Li C, Thiombiano B, Rahimi M, Dong L. 2020. Adaptation of the parasitic plant lifecycle: germination is controlled by essential host signaling molecules. *Plant Physiology* **185**: 1292–1308.

Boyer FD, de Saint Germain A, Pillot JP, Pouvreau JB, Chen VX, Ramos S, Stevenin A, Simier P, Delavault P, Beau JM *et al.* 2012. Structure-activity relationship studies of strigolactone-related molecules for branching inhibition in garden pea: molecule design for shoot branching. *Plant Physiology* **159**: 1524–1544.

Brewer PB, Yoneyama K, Filardo F, Meyers E, Scaffidi A, Frickey T, Akiyama K, Seto Y, Dun EA, Cremer JE *et al.* 2016. *LATERAL BRANCHING OXIDOREDUCTASE* acts in the final stages of strigolactone biosynthesis in *Arabidopsis*. *Proceedings of the National Academy of Sciences, USA* **113**: 6301–6306.

Cankar K, van Houwelingen A, Bosch D, Sonke T, Bouwmeester H, Beekwilder J. 2011. A chicory cytochrome P450 mono-oxygenase CYP71AV8 for the oxidation of (+)-valencene. *FEBS Letters* **585**: 178–182.

Cheng Y, Liu H, Tong X, Liu Z, Zhang X, Li D, Jiang X, Yu X. 2020. Identification and analysis of CYP450 and UGT supergene family members from the transcriptome of *Aralia elata* (Miq.) seem reveal candidate genes for triterpenoid saponin biosynthesis. *BMC Plant Biology* **20**: 214.

Cook CE, Whichard LP, Turner B, Wall ME, Egley GH. 1966. Germination of witchweed (*Striga lutea* Lour.): isolation and properties of a potent stimulant. *Science* **154**: 1189–1190.

Darriba D, Posada D, Kozlov AM, Stamatakis A, Morel B, Flouri T. 2019. ModelTest-NG: a new and scalable tool for the selection of DNA and protein evolutionary models. *Molecular Biology and Evolution* **37**: 291–294.

Dekkers BJ, Willems L, Bassel GW, van Bolderen-Veldkamp R, Ligterink W, Hilhorst HW, Bentsink L. 2012. Identification of reference genes for RT–qPCR expression analysis in *Arabidopsis* and tomato seeds. *Plant and Cell Physiology* **53**: 28–37.

Dor E, Yoneyama K, Wininger S, Kapulnik Y, Yoneyama K, Koltai H, Xie X, Hershenhorn J. 2011. Strigolactone deficiency confers resistance in tomato line *SL-ORT1* to the parasitic weeds *Phelipanche* and *Orobanche* spp. *Phytopathology* **101**: 213–222.

Drummond RS, Martínez-Sánchez NM, Janssen BJ, Templeton KR, Simons JL, Quinn BD, Karunairetnam S, Snowden KC. 2009. Petunia hybrida CAROTENOID CLEAVAGE DIOXYGENASE7 is involved in the production of negative and positive branching signals in petunia. *Plant Physiology* **151**: 1867–1877.

Du H, Ran F, Dong H, Wen J, Li J, Liang Z. 2016. Genome-wide analysis, classification, evolution, and expression analysis of the cytochrome P450 93 family in land plants. *PLoS ONE* **11**: e0165020.

Eramian D, Eswar N, Shen MY, Sali A. 2008. How well can the accuracy of comparative protein structure models be predicted? *Protein Science* **17**: 1881–1893.

Gomez-Roldan V, Fermas S, Brewer PB, Puech-Pages V, Dun EA, Pillot JP, Letisse F, Matusova R, Danoun S, Portais JC *et al.* 2008. Strigolactone inhibition of shoot branching. *Nature* **455**: 189–194.

Grabherr MG, Haas BJ, Yassour M, Levin JZ, Thompson DA, Amit I, Adiconis X, Fan L, Raychowdhury R, Zeng Q *et al.* 2011. Full-length transcriptome assembly from RNA-Seq data without a reference genome. *Nature Biotechnology* **29**: 644–652.

Hansen NL, Miettinen K, Zhao Y, Ignea C, Andreadelli A, Raadam MH, Makris AM, Møller BL, Stærk D, Bak S *et al.* 2020. Integrating pathway elucidation with yeast engineering to produce polpunonic acid the precursor of the anti-obesity agent celastrol. *Microbial Cell Factories* **19**: 15.

Huang AC, Jiang T, Liu Y-X, Bai Y-C, Reed J, Qu B, Goossens A, Nützmann H-W, Bai Y, Osbourn A. 2019. A specialized metabolic network selectively modulates *Arabidopsis* root microbiota. *Science* **364**: eaau6389.

Kapulnik Y, Koltai H. 2014. Strigolactone involvement in root development, response to abiotic stress, and interactions with thebiotic soil environment. *Plant Physiology* **166**: 560–569.

Katoh K, Standley DM. 2013. Mafft multiple sequence alignment software v.7: improvements in performance and usability. *Molecular Biology and Evolution* **30**: 772–780.

Khetkam P, Xie X, Kisugi T, Kim HI, Yoneyama K, Uchida K, Yokota T, Nomura T, Yoneyama K. 2014. 7α-and 7β-Hydroxyorobanchyl acetate as germination stimulants for root parasitic weeds produced by cucumber. *Journal of Pesticide Science* **39**: 121–126.

Kim B, Westerhuis JA, Smilde AK, Floková K, Suleiman AK, Kuramae EE, Bouwmeester HJ, Zancarini A. 2022. Effect of strigolactones on recruitment of the rice root-associated microbiome. *FEMS Microbiology Ecology* **98**: fiac010.

Kohlen W, Charnikhova T, Bours R, López-Ráez JA, Bouwmeester H. 2013. Tomato strigolactones: a more detailed look. *Plant Signaling & Behavior* **8**: e22785.

Kohlen W, Charnikhova T, Lammers M, Pollina T, Tóth P, Haider I, Pozo MJ, de Maagd RA, Ruyter-Spira C, Bouwmeester HJ. 2012. The tomato *CAROTENOID CLEAVAGE DIOXYGENASE 8* (*SlCCD8*) regulates rhizosphere signaling, plant architecture and affects reproductive development through strigolactone biosynthesis. *New Phytologist* **196**: 535–547.

Kohlen W, Charnikhova T, Liu Q, Bours R, Domagalska MA, Beguerie S, Verstappen F, Leyser O, Bouwmeester H, Ruyter-Spira C. 2011. Strigolactones are transported through the xylem and play a key role in shoot architectural response to phosphate deficiency in nonarbuscular mycorrhizal host *Arabidopsis*. *Plant Physiology* **155**: 974–987.

Koltai H, LekKala SP, Bhattacharya C, Mayzlish-Gati E, Resnick N, Wininger S, Dor E, Yoneyama K, Yoneyama K, Hershenhorn J *et al.* 2010. A tomato strigolactone-impaired mutant displays aberrant shoot morphology and plant interactions. *Journal of Experimental Botany* **61**: 1739–1749.

Lin H, Wang R, Qian Q, Yan M, Meng X, Fu Z, Yan C, Jiang B, Su Z, Li J. 2009. DWARF27, an iron-containing protein required for the biosynthesis of strigolactones, regulates rice tiller bud outgrowth. *Plant Cell* **21**: 1512–1525.

Liu Y, Schiff M, Dinesh-Kumar SP. 2002. Virus-induced gene silencing in tomato. *The Plant Journal* **31**: 777–786.

López-Ráez JA, Charnikhova T, Gómez-Roldán V, Matusova R, Kohlen W, De Vos R, Verstappen F, Puech-Pages V, Bécard G, Mulder P *et al.* 2008. Tomato strigolactones are derived from carotenoids and their biosynthesis is promoted by phosphate starvation. *New Phytologist* **178**: 863–874.

Matusova R, Rani K, Verstappen FW, Franssen MC, Beale MH, Bouwmeester HJ. 2005. The strigolactone germination stimulants of the plant-parasitic *Striga* and *Orobanche* spp. are derived from the carotenoid pathway. *Plant Physiology* **139**: 920–934.

Morris SE, Turnbull CG, Murfet IC, Beveridge CA. 2001. Mutational analysis of branching in pea. Evidence that *Rms1* and *Rms5* regulate the same novel signal. *Plant Physiology* **126**: 1205–1213.

Nelson D, Werck-Reichhart D. 2011. A P450-centric view of plant evolution. *The Plant Journal* **66**: 194–211.

Nelson DR, Schuler MA. 2013. Cytochrome P450 genes from the sacred lotus genome. *Tropical Plant Biology* **6**: 138–151.

Nomura S, Nakashima H, Mizutani M, Takikawa H, Sugimoto Y. 2013. Structural requirements of strigolactones for germination induction and inhibition of *Striga gesnerioides* seeds. *Plant Cell Reports* **32**: 829–838.

Oliveros J. 2007. *Venny. An interactive tool for comparing lists with Venn's diagrams.* [WWW document] URL https://bioinfogp.cnb.csic.es/tools/venny/index.html [accessed 14 August 2019].

Pavan S, Schiavulli A, Marcotrigiano AR, Bardaro N, Bracuto V, Ricciardi F, Charnikhova T, Lotti C, Bouwmeester H, Ricciardi L. 2016. Characterization of low-strigolactone germplasm in pea (*Pisum sativum* L.) resistant to *Crenate broomrape* (*Orobanche crenata* Forsk.). *Molecular Plant–Microbe Interactions* **29**: 743–749.

Pompon D, Louerat B, Bronine A, Urban P. 1996. Yeast expression of animal and plant P450s in optimized redox environments. *Methods in Enzymology* **272**: 51–64.

© 2022 The Authors
New Phytologist © 2022 New Phytologist Foundation.

Qin Y, Bai S, Li W, Sun T, Galbraith DW, Yang Z, Zhou Y, Sun G. 2020. Transcriptome analysis reveals key genes involved in the regulation of nicotine biosynthesis at early time points after topping in tobacco (*Nicotiana tabacum* L.). *BMC Plant Biology* **20**: 1–15.

Rani K, Zwanenburg B, Sugimoto Y, Yoneyama K, Bouwmeester HJ. 2008. Biosynthetic considerations could assist the structure elucidation of host plant produced rhizosphere signalling compounds (strigolactones) for arbuscular mycorrhizal fungi and parasitic plants. *Plant Physiology and Biochemistry* **46**: 617–626.

Ronquist F, Huelsenbeck JP. 2003. MrBayes 3: Bayesian phylogenetic inference under mixed models. *Bioinformatics* **19**: 1572–1574.

Ruyter-Spira C, Kohlen W, Charnikhova T, van Zeijl A, van Bezouwen L, de Ruijter N, Cardoso C, Lopez-Raez JA, Matusova R, Bours R *et al.* 2011. Physiological effects of the synthetic strigolactone analog GR24 on root system architecture in *Arabidopsis*: another belowground role for strigolactones? *Plant Physiology* **155**: 721–734.

Salentin S, Schreiber S, Haupt VJ, Adasme MF, Schroeder M. 2015. PLIP: fully automated protein–ligand interaction profiler. *Nucleic Acids Research* **43**: W443–W447.

Seto Y, Sado A, Asami K, Hanada A, Umehara M, Akiyama K, Yamaguchi S. 2014. Carlactone is an endogenous biosynthetic precursor for strigolactones. *Proceedings of the National Academy of Sciences, USA* **111**: 1640–1645.

Simons JL, Napoli CA, Janssen BJ, Plummer KM, Snowden KC. 2007. Analysis of the *DECREASED APICAL DOMINANCE* genes of petunia in the control of axillary branching. *Plant Physiology* **143**: 697–706.

Sohrabi R, Huh J-H, Badieyan S, Rakotondraibe LH, Kliebenstein DJ, Sobrado P, Tholl D. 2015. *In planta* variation of volatile biosynthesis: an alternative biosynthetic route to the formation of the pathogen-induced volatile homoterpene DMNT via triterpene degradation in *Arabidopsis* roots. *Plant Cell* **27**: 874–890.

Sorefan K, Booker J, Haurogné K, Goussot M, Bainbridge K, Foo E, Chatfield S, Ward S, Beveridge C, Rameau C *et al.* 2003. *MAX4* and *RMS1* are orthologous dioxygenase-like genes that regulate shoot branching in *Arabidopsis* and pea. *Genes & Development* **17**: 1469–1474.

Stigliani AL, Giorio G, D'Ambrosio C. 2011. Characterization of P450 carotenoid β-and ε-hydroxylases of tomato and transcriptional regulation of xanthophyll biosynthesis in root, leaf, petal and fruit. *Plant and Cell Physiology* **52**: 851–865.

Sui C, Zhang J, Wei J, Chen S, Li Y, Xu J, Jin Y, Xie C, Gao Z, Chen H *et al.* 2011. Transcriptome analysis of *Bupleurum chinense* focusing on genes involved in the biosynthesis of saikosaponins. *BMC Genomics* **12**: 539.

Sun H, Tao J, Hou M, Huang S, Chen S, Liang Z, Xie T, Wei Y, Xie X, Yoneyama K *et al.* 2015. A strigolactone signal is required for adventitious root formation in rice. *Annals of Botany* **115**: 1155–1162.

Tokunaga T, Hayashi H, Akiyama K. 2015. Medicaol, a strigolactone identified as a putative didehydro-orobanchol isomer, from *Medicago truncatula*. *Phytochemistry* **111**: 91–97.

Trott O, Olson AJ. 2010. AutoDock Vina: improving the speed and accuracy of docking with a new scoring function, efficient optimization, and multithreading. *Journal of Computational Chemistry* **31**: 455–461.

Tzfadia O, Diels T, De Meyer S, Vandepoele K, Aharoni A, Van de Peer Y. 2015. CoExpNetViz: comparative co-expression networks construction and visualization tool. *Frontiers in Plant Science* **6**: 1194.

Umehara M, Hanada A, Yoshida S, Akiyama K, Arite T, Takeda-Kamiya N, Magome H, Kamiya Y, Shirasu K, Yoneyama K *et al.* 2008. Inhibition of shoot branching by new terpenoid plant hormones. *Nature* **455**: 195–200.

Valentine T, Shaw J, Blok VC, Phillips MS, Oparka KJ, Lacomme C. 2004. Efficient virus-induced gene silencing in roots using a modified tobacco rattle virus vector. *Plant Physiology* **136**: 3999–4009.

Vogel JT, Walter MH, Giavalisco P, Lytovchenko A, Kohlen W, Charnikhova T, Simkin AJ, Goulet C, Strack D, Bouwmeester HJ. 2010. *SlCCD7* controls strigolactone biosynthesis, shoot branching and mycorrhiza-induced apocarotenoid formation in tomato. *The Plant Journal* **61**: 300–311.

Wakabayashi T, Hamana M, Mori A, Akiyama R, Ueno K, Osakabe K, Osakabe Y, Suzuki H, Takikawa H, Mizutani M. 2019. Direct conversion of carlactonoic acid to orobanchol by cytochrome P450 *CYP722C* in strigolactone biosynthesis. *Science Advances* **5**: eaax9067.

Wang Y, Bouwmeester HJ. 2018. Structural diversity in the strigolactones. *Journal of Experimental Botany* **69**: 2219–2230.

Wang Y, Duran HGS, van Haarst JC, Schijlen EGWM, Ruyter-Spira C, Medema MH, Dong L, Bouwmeester HJ. 2021. The role of strigolactones in P deficiency induced transcriptional changes in tomato roots. *BMC Plant Biology* **21**: 349.

Webb B, Sali A. 2016. Comparative protein structure modeling using Modeller. *Current Protocols in Bioinformatics* **54**: 5.6.1–5.6.37.

Werck-Reichhart D, Feyereisen R. 2000. Cytochromes P450: a success story. *Genome Biology* **1**: reviews3003.3001.

Xie X. 2016. Structural diversity of strigolactones and their distribution in the plant kingdom. *Journal of Pesticide Science* **41**: 175–180.

Xie X, Mori N, Yoneyama K, Nomura T, Uchida K, Yoneyama K, Akiyama K. 2019. Lotuslactone, a non-canonical strigolactone from *Lotus japonicus*. *Phytochemistry* **157**: 200–205.

Xie X, Yoneyama K, Kisugi T, Uchida K, Ito S, Akiyama K, Hayashi H, Yokota T, Nomura T, Yoneyama K. 2013. Confirming stereochemical structures of strigolactones produced by rice and tobacco. *Molecular Plant* **6**: 153–163.

Xie X, Yoneyama K, Yoneyama K. 2010. The strigolactone story. *Annual Review of Phytopathology* **48**: 93–117.

Xu X, Fang P, Zhang H, Chi C, Song L, Xia X, Shi K, Zhou Y, Zhou J, Yu J. 2018. Strigolactones positively regulate defense against root-knot nematodes in tomato. *Journal of Experimental Botany* **70**: 1325–1337.

Xu X, Jibran R, Wang Y, Dong L, Flokova K, Esfandiari A, McLachlan ARG, Heiser A, Sutherland-Smith AJ, Brummell DA *et al.* 2021. Strigolactones regulate sepal senescence in Arabidopsis. *Journal of Experimental Botany* **72**: 5462–5477.

Yoneyama K, Ruyter-Spira C, Bouwmeester H. 2013. Induction of germination. In: Joel DM, Gressel J, Musselman LJ, eds. *Parasitic Orobanchaceae: parasitic mechanisms and control strategies*. Berlin & Heidelberg, Germany: Springer, 167–194.

Yoneyama K, Xie X, Kisugi T, Nomura T, Sekimoto H, Yokota T, Yoneyama K. 2011. Characterization of strigolactones exuded by Asteraceae plants. *Plant Growth Regulation* **65**: 495–504.

Yoneyama K, Xie X, Sekimoto H, Takeuchi Y, Ogasawara S, Akiyama K, Hayashi H, Yoneyama K. 2008. Strigolactones, host recognition signals for root parasitic plants and arbuscular mycorrhizal fungi, from Fabaceae plants. *New Phytologist* **179**: 484–494.

Zhang Y, Cheng X, Wang Y, Díez-Simón C, Flokova K, Bimbo A, Bouwmeester HJ, Ruyter-Spira C. 2018. The tomato MAX1 homolog, SlMAX1, is involved in the biosynthesis of tomato strigolactones from carlactone. *New Phytologist* **219**: 297–309.

Zhang Y, Van Dijk AD, Scaffidi A, Flematti GR, Hofmann M, Charnikhova T, Verstappen F, Hepworth J, Van Der Krol S, Leyser O. 2014. Rice cytochrome P450 MAX1 homologs catalyze distinct steps in strigolactone biosynthesis. *Nature Chemical Biology* **10**: 1028–1033.

Zou J, Zhang S, Zhang W, Li G, Chen Z, Zhai W, Zhao X, Pan X, Xie Q, Zhu L. 2006. The rice *HIGH-TILLERING DWARF1* encoding an ortholog of *Arabidopsis* MAX3 is required for negative regulation of the outgrowth of axillary buds. *The Plant Journal* **48**: 687–698.

Zwanenburg B, Pospíšil T. 2013. Structure and activity of strigolactones: new plant hormones with a rich future. *Molecular Plant* **6**: 38–62.

Supporting Information

Additional Supporting Information may be found online in the Supporting Information section at the end of the article.

Dataset S1 Homologous protein sequences of *CYP712* gene family in 14 species across the flowering plants.

Dataset S2 Binding energies returned using AutoDock Vina for the best conformation in each docking run.

© 2022 The Authors
New Phytologist © 2022 New Phytologist Foundation.

Fig. S1 Design of RNA-seq experiment in wild-type tomato and *SlCCD8* RNAi line.

Fig. S2 Alignments to templates for CYP712G1 from *Solanum lycopersicum*, CYP712B from *Medicago truncatula*, and two tobacco CYP712G1 length variants: short and long.

Fig. S3 The production of strigolactones in tomato was induced by P starvation.

Fig. S4 The expression of strigolactone biosynthetic genes in tomato plants of the RNA-seq experiment.

Fig. S5 *Nicotiana benthamiana* infiltration with orobanchol pathway and P450 candidate genes.

Fig. S6 Multiple reaction monitoring chromatograms of didehydro-orobanchol isomers produced in yeast microsome assays and analysed using LC–MS on a C18 column.

Fig. S7 Multiple reaction monitoring chromatograms of hydroxy-orobanchol and orobanchol in yeast microsome *in vitro* assay and tomato root exudate.

Fig. S8 Putative biosynthetic pathways of solanacol in tomato.

Fig. S9 Quantification of strigolactones in assays with yeast microsomes expressing *CYP712G1* incubated with orobanchol in a time series.

Fig. S10 Homology models of CYP712G1 from *Solanum lycopersicum*, CYP712B from *Medicago truncatula*, and two tobacco CYP712G1 length variants: short and long.

Fig. S11 Chromatogram of didehydro-orobanchol isomers and hydroxy-orobanchol in yeast microsome *in vitro* assay with mutated *CYP712G1*.

Fig. S12 Phylogenetic tree of CYP712 and CYP705 amino acid sequences showing two main clades.

Fig. S13 Hydroxy-orobanchol in tomato root exudate and produced by yeast microsomes from orobanchol.

Fig. S14 Hydroxy-orobanchol produced in tomato root exudate, produced by yeast microsomes from orobanchol and in *N. benthamiana* transient expression.

Fig. S15 Docking of *Medicago* CYP712B and tobacco CYP712G1 length variants with orobanchol, 2′-epi-orobanchol, ent-orobanchol, and ent-2′-epi-orobanchol.

Table S1 The sequence of CYP712G1 and its mutants.

Table S2 Primers used in this study.

Table S3 Pearson correlation coefficients for candidate genes and baits.

Please note: Wiley Blackwell are not responsible for the content or functionality of any Supporting Information supplied by the authors. Any queries (other than missing material) should be directed to the *New Phytologist* Central Office.

© 2022 The Authors
New Phytologist © 2022 New Phytologist Foundation.